PSD flux database and analysis

Ludovic Bariteau
Chris Fairall

December 2016

I) Description of the database

For the purpose of this project, two flux database were compiled. The flux data file FluxBase_1hr_v12192016.txt is the release of the hourly database that incorporates the historical data from 12 cruises done in the 1990's (Fairall et al., 2003) and from 10 cruises of the PACS/EPIC dataset. In addition to this, data from 19 cruises were added yielding a database containing about 41 cruises spanning over 25 years (as of September 2016). Figure 1 shows the tracks of all the cruises from which data have been appended in the database.

The second file, FluxBase_10min_12192016.txt, contains 10-min data form about 20 most recent cruises (2004 to 2016) as this data are retrievable. Unfortunately it is near impossible to retrieve all the raw or 10-min data from the 1990's cruises.

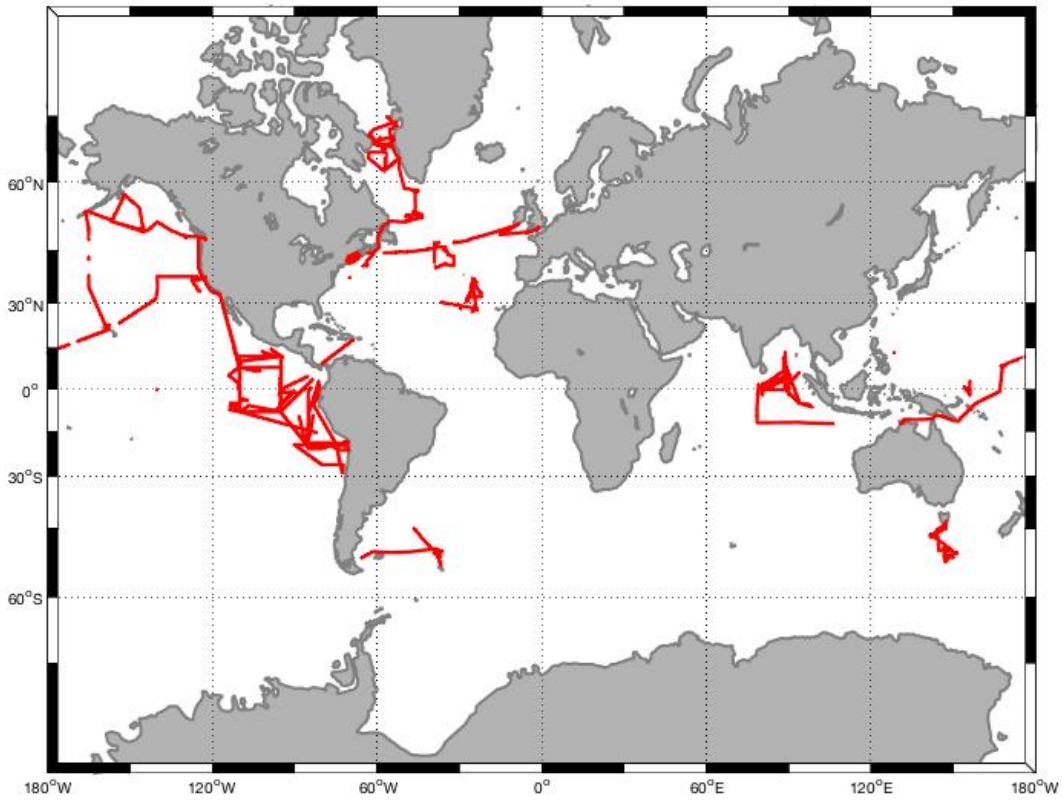

Figure 1. *Cruise tracks for 41 PSD projects from 1990 through 2016.*

Both files have a similar format and for now follow historical formatting from ETL cruise database. They contain turbulent and radiative fluxes plus bulk meteorological variables as well as bulk estimates of the turbulent fluxes computed using the recently updated 3.5 version of the COARE flux algorithm (see Edson et al., 2013 for more information). Most quantities have been subjected to one round of intercomparison/calibration scrutiny; however, there may be future modifications. When covariance could not be computed, columns were filled with NaN's (Not a Number).

The files are 60 columns; following the decimal day-of-year, the next 10 columns are mean variables from the PSD system (except column 7 which is a mix of both the ship and PSD's systems); columns 39-46 are similar data from the ships sensors. Columns 12-21 are turbulent fluxes the last 8 columns (covariance, ID, and bulk); columns 22-23 the radiative fluxes and 24 the rain rate. Columns 25-27 are turbulence data quality indicators; 28-31 turbulent structure function parameters (indices of small-scale turbulence in the inertial subrange). Columns 32-33 are the minor (rain and Webb) heat flux components; 34-35 the latitude and longitude; 36-38 the heights of the PSD wind, temperature, and humidity mean sensors. Columns 47-49 are other mean variables from the PSD system, like the atmospheric pressure and relative humidity. Columns 50-53 are energy budget related variables. Column 54 is the year when the measurements occurred and column 55 is an ascii code indicative of the cruise name project. Finally columns 57-60 are variances of some PSD variables. The 10-min file has some structure coefficients at the end of the file adding 8 extra columns

If using MATLAB, the data can be directly acquired with a 'impordata' statement.

```
x=importdata('your local directory/FluxBase_1hr_v10052016.txt');
jdyx=x(:,1);%fractional (decimal) day-of-year
ushp=x(:,2);%doppler log, ship sensor (m/s) – when not available set to zero or replaced by SOG.
U=x(:,3);%true wind speed, PSD sonic (m/s)
dir=x(:,4);%true wind direction, PSD sonic (deg)
urel=x(:,5);%relative wind speed, PSD sonic (m/s)
reldir=x(:,6);%relative wind direction, PSD sonic (deg from bow)
head=x(:,7);%ship heading (deg clockwise rel. north) – PSD or ship
tsnk=x(:,8);%sea snake temperature, PSD, 0.05 m depth (C)
ta=x(:,9);%air temperature, PSD (C)
qse=x(:,10);%sea surface specific humidity, from snake (g/kg)
qa=x(:,11);%air specific humidity, PSD (g/kg)
hsc=x(:,12);%sensible heat flux, covariance (W/m^2)
hsib=x(:,13);%sensible heat flux, ID (W/m^2)
hsb=x(:,14);%bulk sensible heat flux, (W/m^2)
hlc=x(:,15);%latent heat flux, covariance, (W/m^2)
hlib=x(:,16);%latent heat flux, ID, (W/m^2)
hlb=x(:,17);%bulk latent heat flux, W/m^2 (includes Webb et al. correction)
taucx=x(:,18);%covariance streamwise stress (N/m^2)
taucy=x(:,19);%covariance cross-stream stress (N/m^2)
tauib=x(:,20);%ID streamwise stress (N/m^2)
taub=x(:,21);%bulk wind stress along mean wind, (N/m^2)
rs=x(:,22);%downward solar flux (W/m^2)
rl=x(:,23);%downward IR flux (W/m^2)
org=x(:,24);%rainrate, PSD STI optical rain gauge, uncorrected (mm/hr)
J=x(:,25);%ship plume contamination index
tiltx=x(:,26);%flow tilt at PSD sonic anemometer, earth frame (deg)
Jm=x(:,27);%ship maneuver index
ct=x(:,28);%ct^2 (K^2/m^.667)
cq=x(:,29);%cq^2 ((g/kg)^2/m^.667)
cu=x(:,30);%cu^2 ((m/s)^2/m^.667)
cw=x(:,31);%cw^2 ((m/s)^2/m^.667)
hrain=x(:,32);%rain heat flux, Gosnell et al 1995 (W/m^2)
hlwebb=x(:,33);%correction to measured latent heat flux, Webb et al.
lat=x(:,34);%latitude (deg)
lon=x(:,35);%longitude (deg)
```

```
zu=x(:,36);%wind speed measurement height (m)
zt=x(:,37);%air temperature measurement height (m)
zq=x(:,38);% air humidity measurement height (m)
sog=x(:,39);%speed over ground, ship GPS (m/s)
U_scs=x(:,40); %true wind speed, ship anemometer (m/s)
dir_scs=x(:,41);%true wind direction, ship anemometer (deg)
cog=x(:,42);%course over ground, ship gps (m/s)
tsg=x(:,43);%ship water temperature, ~5 m depth, (C)
ta_im=x(:,44);%ship air temperature (C)
qs_tsg=x(:,45);%ship bulk water specific humidity (g/kg)
qa_im=x(:,46);%ship air specific humidity, (g/kg)
press=x(:,47);                %PSD atmospheric pressure, (mbar) – set to 1010mbar when not measured
RH=x(:,48); %PSD RH (%)
qlic=x(:,49); % Specific Humidity from Licor (g/kg)
rlcler=x(:,50);% Longwave downwelling clear sky model (W/m2)
Rscl=x(:,51); % Shortwave solar radiance clear sky model (W/m2)
rnl=x(:,52); % net longwave heat flux
hnet=x(:,53);% net heat flux, bulk, W/m2
year=x(:,54);%project year
pcode=x(:,55); %project code;  % Metz =  77; Epic = 69; WHOTS = 87; STRATUS = 83; NEAQS = 78; HiWInGS = 72;
GasEx = 71
% DYNAMO = 68; Calwater = 67; Capricorn = 73;
uuj=x(:,56);  `%variance of u (m/s)
vvj=x(:,57);  %variance of v (m/s)
wwj=x(:,58);  %variance of w (m/s)
tt=x(:,59);   %variance of t (degC)
qq=x(:,60);   %std of q  (g/kg)
```

The 10-min database is the same as above but with 8 more columns:

```
Cu_a =   x(:,61);    % cu^2 U method a
Cu_b=   x(:,62);    % cu^2 U method b
Cw_a =   x(:,63);   % cw^2 W method a
Cw_b =   x(:,64);   % cw^2 W method b
Ct_a=   x(:,65);   % ct^2 temperature method a
Ct_b =   x(:,66);   % ct^2 temperature method b
Cq_a =   x(:,67);   % cq^2 H2O Licor method a
Cq_b  =   x(:,68);   % cq^2 H2O Licor method b
```

Further experimental details are as follows:

* A correction scheme was applied to the measurement made from the Windmaster sonic (pre-2015 versions). The scheme follows Nakai 2012.

* The values given for covariance and ID latent heat fluxes in the file are Le<w' rho_v'>. Values for hl_webb are included in column 33. This should be applied to the covariance and Inertial Dissipatio (ID) values (Hlatent = Le <w' rho_v'> + hl_webb). It is already included in the bulk values given here.

*A correction to account for biases in gas concentration measurements has been applied on the covariance and ID latent heat fluxes. See Fratini et al. 2014 for more details.

* Sensible heat flux was computed from vertical velocity - sonic temperature covariance. The humidity contribution to sonic temperature was removed using the bulk latent heat flux.

* Simple data quality indicators have been used to edit the turbulence data. In averaging to one-hr averages, values for covariance and ID turbulence variables were computed if the following criteria were met:

jj=find((reldir<60 | reldir>300) & J==0 & Jm<3 & org<5) (1)

with:

- *reldir* is the relative wind direction
- A value of *J*=0 implies no ship contamination.
- A value of *Jm*<3 implies no significant maneuver during the average.
- *org* is the rainrate

If there were no valid values in the 1-hr interval, the turbulence variables were set to NaN. Note that these filters were adjusted from project to project. For instance the relative wind direction was setup to [90,270] in earlier cruises. To be consistent, once the data are loaded, we apply the filters on the entire database and constrain the relative direction to +/- 60deg from the bow. We also add a constrain on the mean ship speed by using ushp<3.5.

* Data from the 2004 New England Air Quality Study (NEAQS-04) are included in this dataset but it has to be noted that during that project we found significant suppression of the transfer coefficients for momentum, sensible heat, and latent heat; mainly because our measurements at 18-m height did not realize the full surface flux in these shallower boundary layer conditions. (Fairall et al., 2006).

II) Flux analysis and COARE 3.5

As a quality check of the database, we run the standard flux and transfer coefficient program developed for the COARE 3.5 paper (Edson et al. 2013) and compare it against the measured ID and covariance fluxes.

Results below are shown for the grand average properties (stress/Cd – 8467 hourly samples; Hlatent/Ce – 5823 hourly samples). In addition to the filtering done in (1), the stress data were also restricted with flow tilt less than 15deg.

Figures 2 shows the individual stress components as a function of the bulk stress. There is a significant cross-stream stress but it is sufficiently small such that the magnitude of the stress vector is essentially the same as the streamwise component. The stress- wind vector difference is 7 degrees. Taking the average of the covariance and ID values yield almost a 1:1 ratio with the Bulk.

Figure 3 shows that 10-m neutral drag coefficient as a function of wind speed. The drag coefficient compares reasonably well with the COARE values.

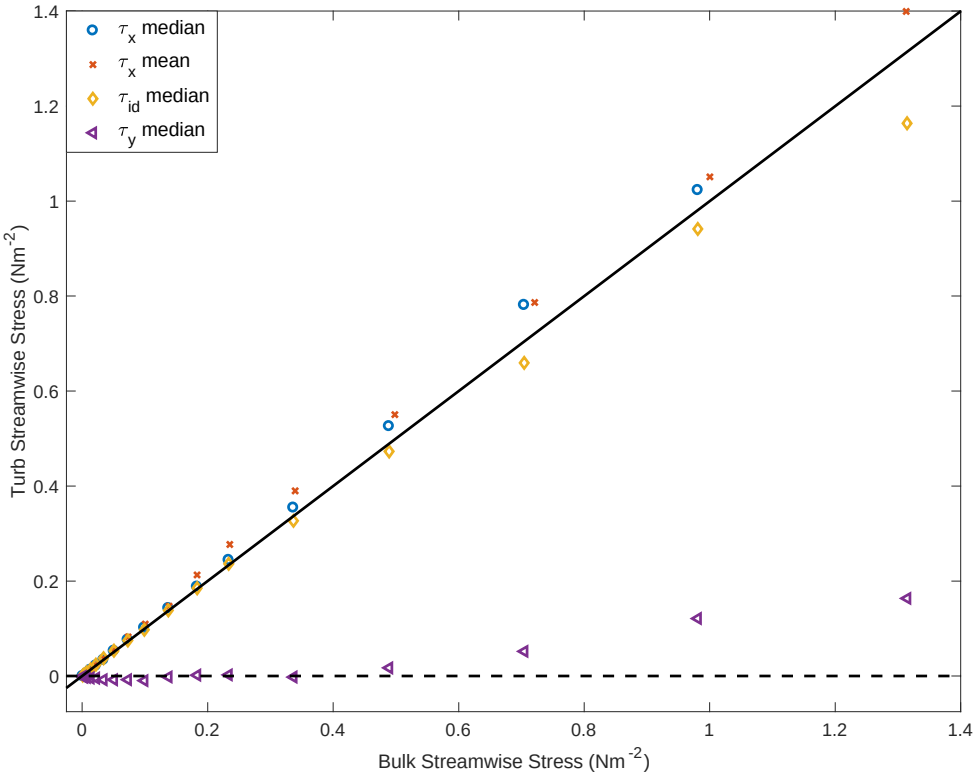

Figure 2. *The average of covariance and ID stress computed in 10-m neutral wind speed bins plotted as a function of bulk stress. The 'x' and 'o' symbols are the means and medians respectively of the streamwise component; the diamonds are the ID values and the triangles are the medians of the cross-stream stress component. The solid line is 1:1.*

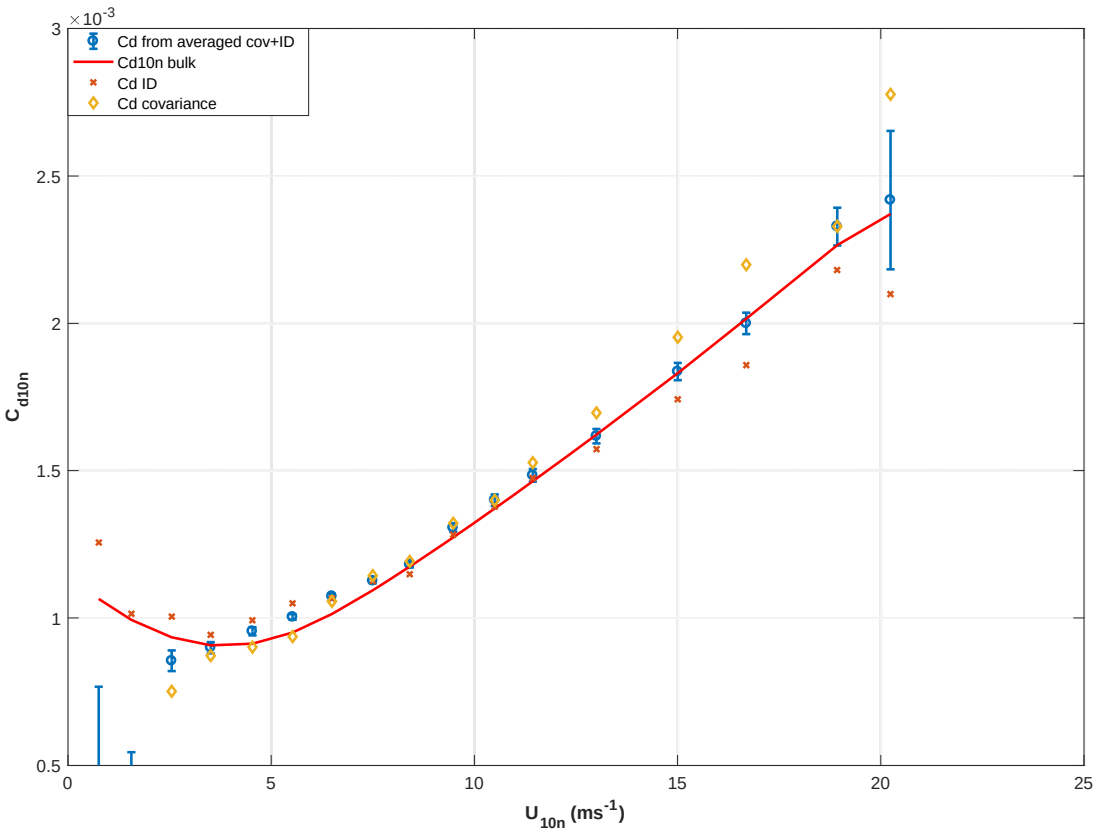

Figure 3. *Median 10-m neutral velocity transfer coefficient as a function of 10-m neutral wind. The 'o' symbols represent the covariance and ID values combined and use Eq. (33) in Fairall 2003. Error bars indicate the one-sigma standard error of the bin median based on the distribution within the mean wind speed bin. The 'x' symbols represent the ID values only; the diamonds the covariance values only. The solid line is COARE 3.5.*

Latent heat flux data were similarly restricted but with a rainrate less than 1mm/hr and a sea-air specific humidity difference greater than 2 g/kg to ensure a good SNR and to edit out contamination of the LiCor7500.

Figures 4 and 5 show similar results for latent heat (a mean of covariance and ID values was used for the direct measurements). Below wind speeds of 7m/s, the neutral 10-m moisture transfer coefficient is about 5% lower than the COARE value. Above 7m/s, the coefficient is about 5% higher than the COARE value. Note however that this difference is very sensitive to the filtering applied and whether we use a combination of means and medians.

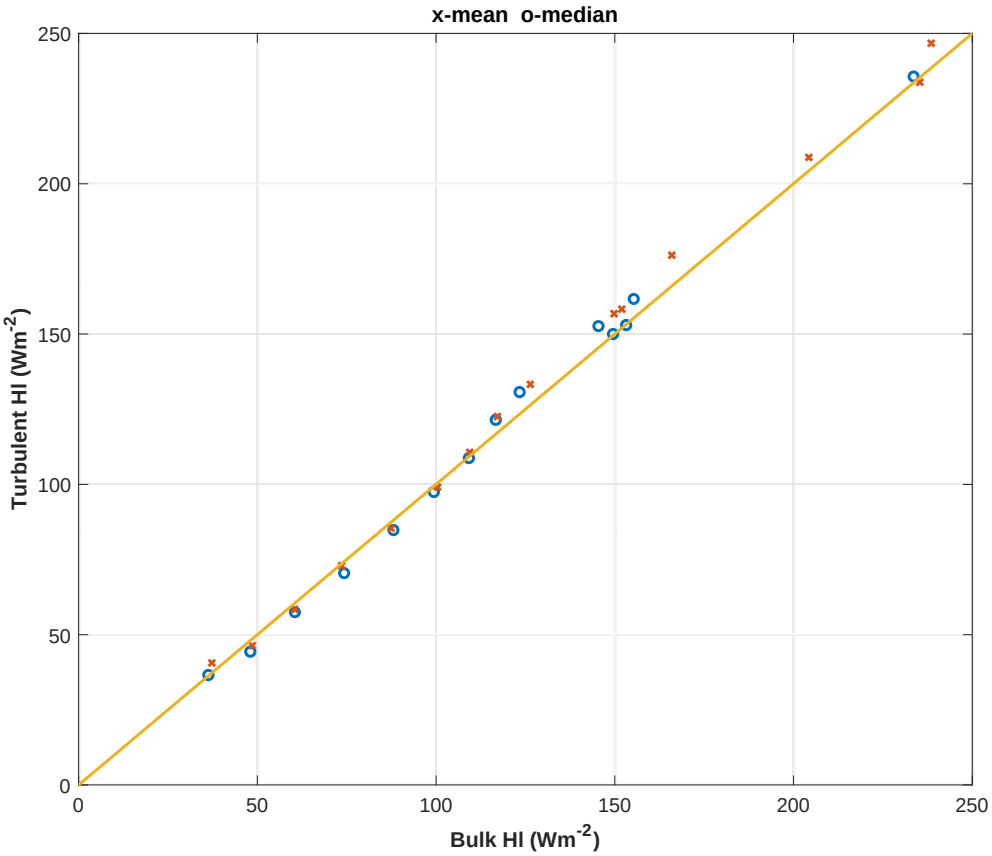

Figure 4. *The average of covariance and ID latent heat fluxes computed in 10-m neutral wind speed bins plotted as a function of bulk latent heat flux. The 'x' symbols are the means; the 'o' are medians, the solid line is 1:1.*

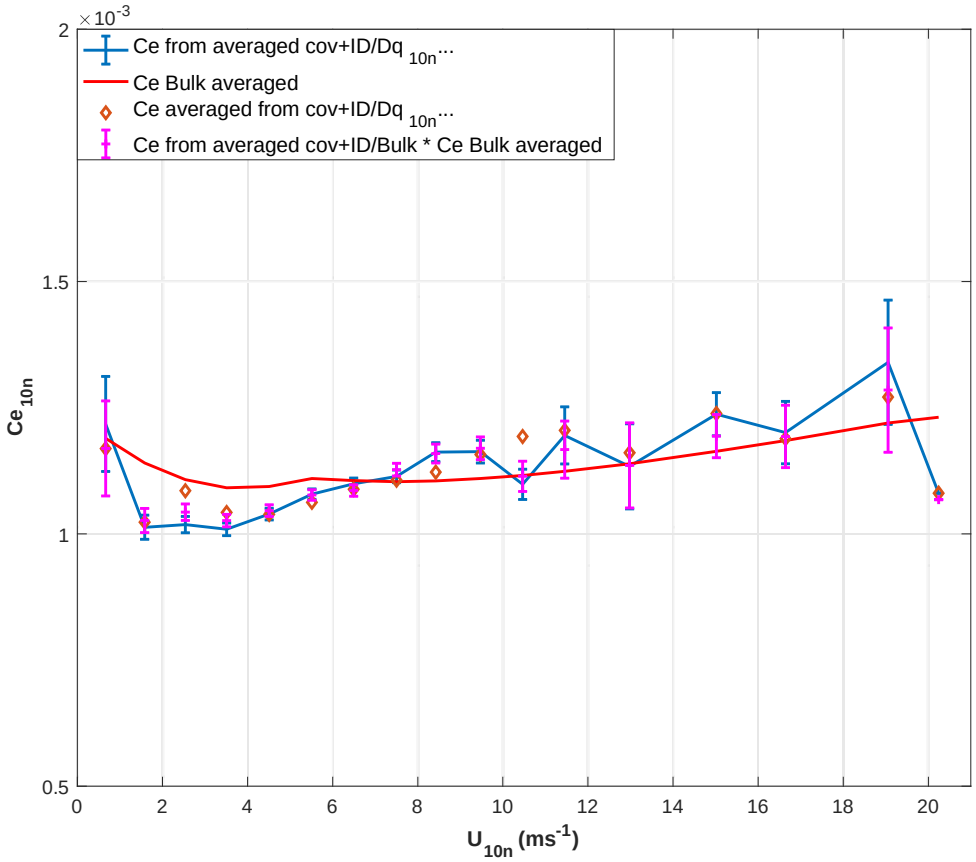

Figure 5. *The 10-m neutral transfer coefficient for moisture as a function of 10-m neutral wind. Error bars indicate the one-sigma standard error of the bin median based on the distribution within the mean wind speed bin. The '+' magenta symbols represent the median of the covariance and ID values and use Eq. (33) in Fairall 2003. The diamonds are the straightforward method, i.e the bin-averaged coefficients computed for each 1-h observation. The blue line is simply using bin-average values of the individual quantities (Eq. (30) in Fairall 2003) and then computes the coefficients. The solid line is COARE 3.5.*

III) Theoretical relationship for sampling uncertainty and averaging length

III.1) Standard deviation

First we look at the atmospheric stability dependence of the standard deviation σ of wind components and some scalars c. Monin-Obhukov similarity scaling may be used to show the stability dependence of variances through the following relationships:

$$\sigma_w = 1.25 u_* f_w(z/L) \qquad (2a)$$

$$\sigma_c = \frac{\overline{wc}}{u_*} 3.0 f_c(z/L) \qquad (3a)$$

$$\sigma_u = 2.39 u_* f_u(z/L) \qquad (4a)$$

where L is the Obukhov length in meters, z the measurement height, u_* is the friction velocity and $\overline{wc}$ is the covariance flux. The f functions are similarity relationships describing the dependence with z/L:

$$f_w(z/L) = [1 + 3\text{abs}(z/L)]^{1/3} \quad z/L<0 \qquad (2b)$$

$$f_w(z/L) = 1 + 0.2z/L \quad z/L>0 \qquad (2c)$$

$$f_c(z/L) = [1 + 20\text{abs}(z/L)]^{-1/3} \quad z/L<0 \qquad (3b)$$

$$f_c(z/L) = 1 + 1.0(z/L)^{1/2} \quad z/L>0 \qquad (3c)$$

$$f_u(z/L) = [1 + 0.12\text{abs}(z_i/L)^{2/3}]^{1/2} \quad z/L<0 \qquad (4b)$$

$$f_u(z/L) = 1 \quad z/L>0 \qquad (4c)$$

Note that for the case of the horizontal velocity components, the dependence is a function of z_i, the depth of the atmospheric mixed layer.

Observations of dimensionless variances are plotted in figures 6, 7 and 8 and compared to the mathematical representations above. The plots are obtained by separating the data into stability bins and computing the mean and standard deviation of the turbulence characteristics. Note that here the standard deviation is computed by taking the half-width at half-max of the distribution to reject the effect of outliers on the standard deviation.

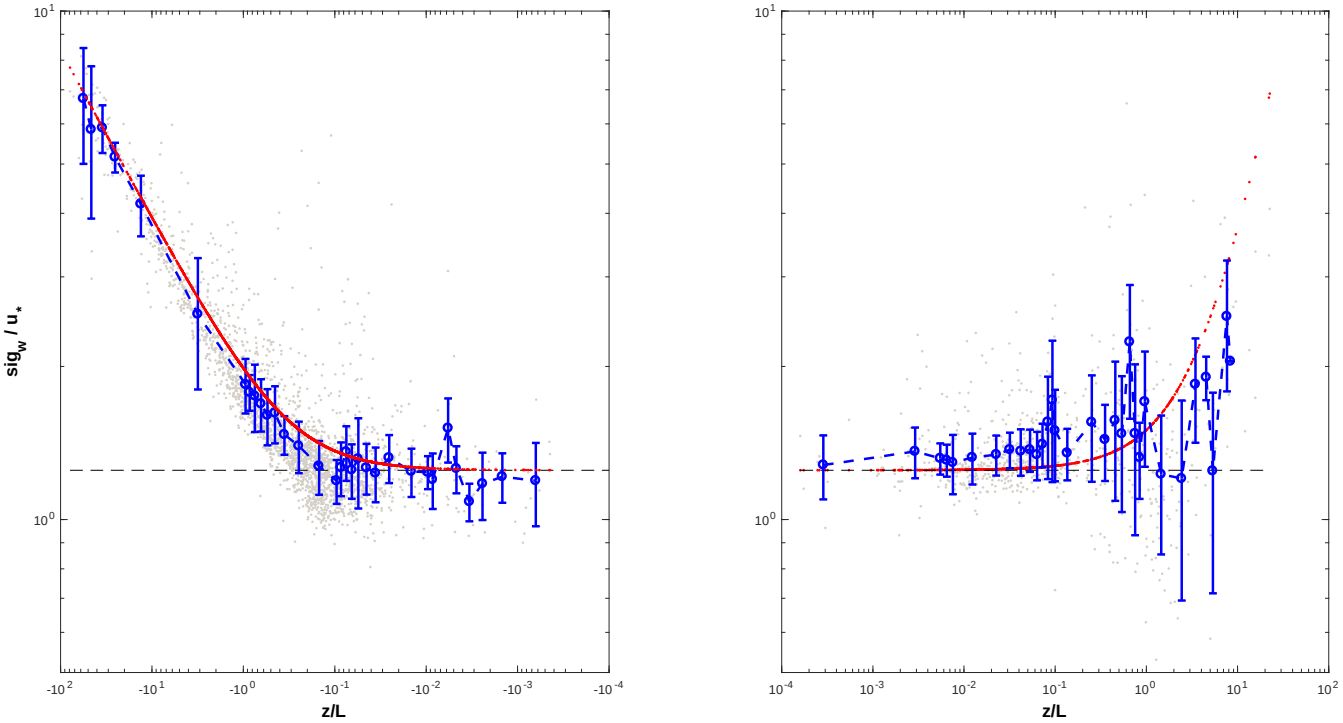

Figure 6. *Dimensionless vertical velocity standard deviation versus stability, z/L: left panel, unstable conditions (z/L<0) and right panel, stable conditions (z/L>0). The grey dots are all the data and the blue circles are the bin-averages mean values. Error bars indicate the one-sigma uncertainty of the bin mean based on the distribution within the mean stability bin. Red lines are mathematical representations using Eq. 2a, 2b and 2c.*

There is a good fit between the unstable stability functions and the observations for vertical velocity. The agreement is a little more finicky in stable air as both σ_w and u_* become small so their ratio is poorly determined and the uncertainty thus larger. For high values of z/L the theoretical ratio appears to increase faster than the observed measurements.

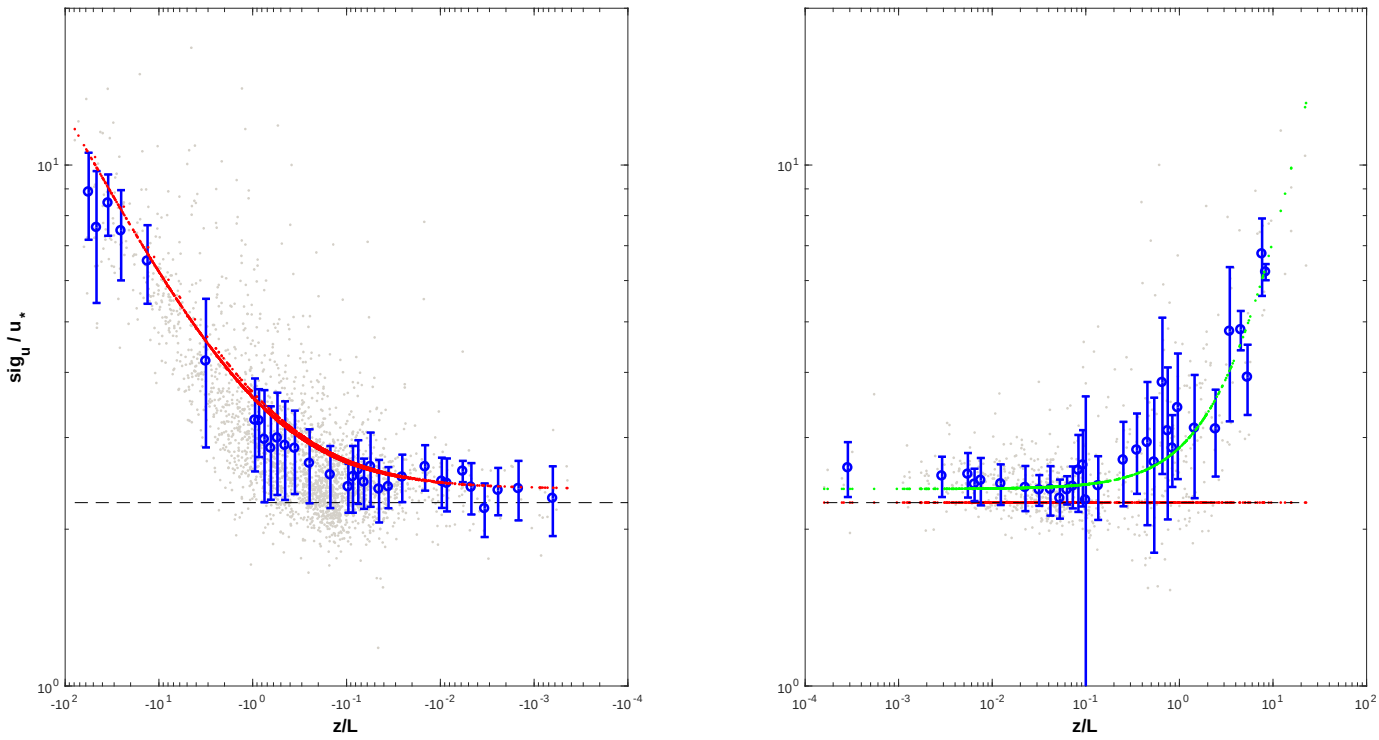

Figure 7. *Dimensionless horizontal velocity u-component standard deviation versus stability, z/L: left panel, unstable conditions (z/L<0) and right panel, stable conditions (z/L>0). The grey dots are all the data and the blue circles are the bin-averages mean values. Error bars indicate the one-sigma uncertainty of the bin mean based on the distribution within the mean stability bin. Red lines are mathematical representations using Eq. 4a, 4b and 4c. The green line on the stable side is Eq. 2c.*

Similarly, there is a good fit between the unstable stability functions and the observations for *u*. On the stable side however the behavior does not seem to be constant but instead behave in the same way as σ_w/u_*, i.e. for very large z/L (strong stability and weak winds) the ratio increases again.

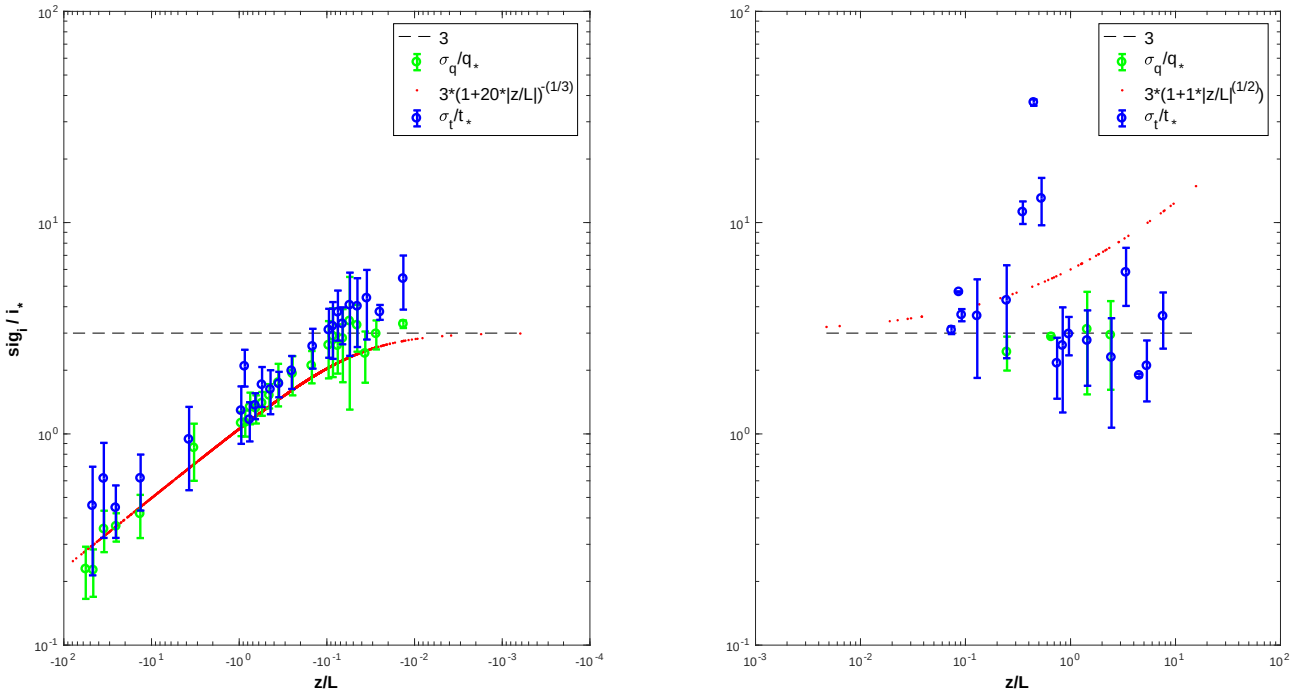

Figure 7. *Dimensionless scalar standard deviation versus stability, z/L: left panel, unstable conditions (z/L<0) and right panel, stable conditions (z/L>0). Blue color is for temperature and green for humidity. Error bars indicate the one-sigma uncertainty of the bin mean based on the distribution within the mean stability bin. Red lines are mathematical representations using Eq. 3a, 3b and 3c.*

In addition to the regular filtering, the temperature and humidity scalars were plotted only for an air-sea ΔT and ΔQ superior to 2 (degC and g/kg respectively). This ensures a good SNR and excludes poorly determined ratio. On the unstable side, the scalar similarity relationship is a descent fit to the humidity scalar and reaches a neutral value near 3. For temperature however it seems the neutral value is slightly higher, somewhere between 4 and 5. This could be an observational issue or simply indicating that humidity and temperature don't behave the same way as scalars.
In stable air, beside some outliers, both scalars appear relatively constant.

III.2) Flux random error

Sampling error remains one of the largest sources of uncertainty on flux measurements and can be expressed as the variance of the eddy-correlation measurement, i.e. the variance of the covariance. Following an approach suggested by Lumley and Panofsky (1964) and later applied by Wyngaard (1973), the flux random error estimate can be approximated by using the instantaneous flux statistics:

$$\delta(\overline{wx}) = \sqrt{\frac{2\tau_i}{T}\left(\overline{wx^2} - \overline{wx}^2\right)} \qquad (5)$$

Here T is the averaging time required to determine the mean flux $\overline{wx}^2$ to an accuracy $\delta(\overline{wx})$, $(\overline{wx^2} - \overline{wx}^2)$ is the ensemble variance of the flux, and τ_i is the integral (decorrelation) time scale of the time function. τ_i can be obtained by integrating the autocorrelation function but some assumptions are commonly made to get an estimate of it as a function of z/U and the cospectra (see below). Another hypothesis commonly made here is that the joint Gaussianity of the individual fluctuations is in reasonable agreement with the flux measurements in the fully turbulent part of the boundary layer. These assumptions are what lead to the expression used by Blomquist et al. (2010) which state that if we take observations of vertical velocity, w, and fluctuations of some scalar constituent, c, over a time period T, then a computation of the covariance of the two variables will be an estimate of the 'true' local ensemble mean of the flux with an uncertainty approximated by

$$\delta(\overline{wc}) = \frac{a\sigma_w\sigma_c}{\sqrt{T / \min(\tau_w, \tau_c)}} \qquad (6)$$

where σ is the standard deviation and can be estimated from Eq. 2 to 4, a is a constant between 1 and 2 (Fairall et al. 2000), and τ is the integral time scale. The constant a reflects the uncertain nature of the relationship arising from approximations to the form of the autocorrelation functions and the interactions of the two variables.

Because there are two variables here, there are two time scales. It is usually postulated that the appropriate time scale is the shorter of the two or the square root of the product of the two τ_{wc}:

$$\min(\tau_w, \tau_c) = \tau_{wc} = b\frac{z}{U_r} f_\tau(z / L) \qquad (7)$$

with b a constant of 2.8, U_r the relative wind speed, and

$$f_\tau(z / L) = [\min(5, \max(0.5, 1 + 0.6 * \mathrm{z/L}))]^{-1} \qquad (8)$$

Usually we can assume the wind speed measurement is relatively noise-free, but the scalar measurement is often subject to various sources of variance. Therefore (5) can be expanded to the following form (see Blomquist et al. 2010):

$$\delta(\overline{wc}) = \frac{a\sigma_w\sigma_c}{\sqrt{T / \tau_{wc}}}\left[1 + \frac{\phi_{wn}}{4\sigma_c^2\tau_{wc}}\right]^{1/2} \qquad (9)$$

where ϕ_{wn} is a constant variance-spectral value for white noise. The noise could be simply electronic or Poisson counting statistics.

To assess the flux error of our database, we first start by verifying the variability of the integral time scale τ as a function of z/L. Fairall studied this during the SCOPE field program (Eq. 8), but we verify this with the most recent cruises. For this, we evaluate the dependence of the location of the cospectral peak, n_m, on stability by finding the maximum of the function $y = ax/(1+bx)^c$ fitted to the normalized cospectrum for

each 10-min period of the most recent cruises (post-2004). This approach is using the universal curves based on Kaimal et al. (1972) but we allow the power coefficient to vary and use it as a quality criterion to reject cospectra that deviate too much from the expected theoretical shape. Usually the coefficient *c* is about 7/3 for *wu* cospectra for instance. On average the fit of the wu cospectra could be expressed as $14.7n/(1+11.1n)^{2.2}$ which is close to what can be found in the literature. Note also that we perform this calculation using the nondimensionalized frequency $n_m=fz/u_r$ to account for the fact that the spectrum shift as the relative wind speed u_r varies. The gustiness effect (discussed later) was also included in this study.

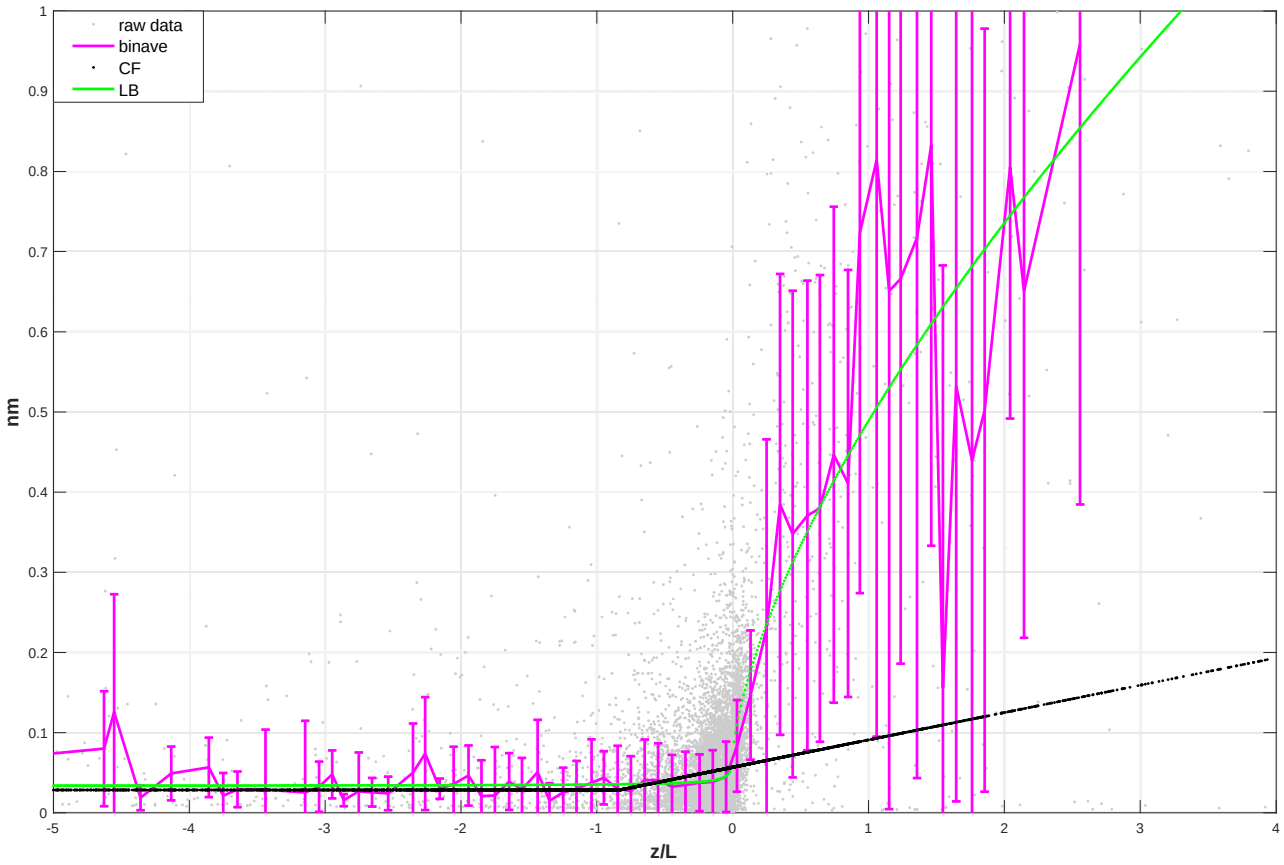

Figure 8. *Nondimensionalized frequency at the cospectral maxima* ($n_m=f_mz/u$) *shown as a function of z/L. Grey dots represent the original data for 10-min periods; magenta solid line - the median value of* n_m *in stability bands; black line – the fitted function using Eq. 8; green line – fitted function of the form using Eq.10a and 10b.*

We can see a rather large scatter in the individual results so an average of the data by stability bins was used. We note that in unstable air (z/L<0) there is little, if any, variation with z/L and that the original formulation in Eq 8. is in the bulk part. In stable cases (z/L>0) the observed trend is higher than the original formulation. For improvements, we use a fit (green line) of the form

$$n_m(z/L) = A1 + \frac{1}{A2 + A3\left|\frac{z}{L}\right|^{2/3}} \qquad z/L<0 \qquad (10a)$$

$$n_m(z/L) = B1 + B2\left(\frac{z}{L}\right)^{2/3} \qquad z/L>0 \qquad (10b)$$

The empirical coefficients A_i and B_i are given in Table 1. We note that the variability of n_m for *wu* is less rapid than for the products *wt* or *wq*. The corresponding integral time scale τ is then computed as:

$$\tau = \frac{z}{2\pi U_r} n_m(z/L)^{-1} \qquad (11)$$

Here U_r should include the gustiness correction. Near neutral conditions, τ is about 2s for wt and wq and 3s for wu while Equation 8. Predicted 4s for all variables.

	z/L<0			z/L>0	
	A1	**A2**	**A3**	**B1**	**B2**
$n_{m,\,wu}$	0.033	25	400	0.069	0.42
$n_{m,\,wt}$	0.06	13	120	0.134	0.16
$n_{m,\,wq}$	0.06	33	120	0.089	0.2

Table 1. *Empirical coefficients of the function in Eq. 10a and 10b fitted to the median values of the cospectral peak location, n_m, on the stability z/L.*

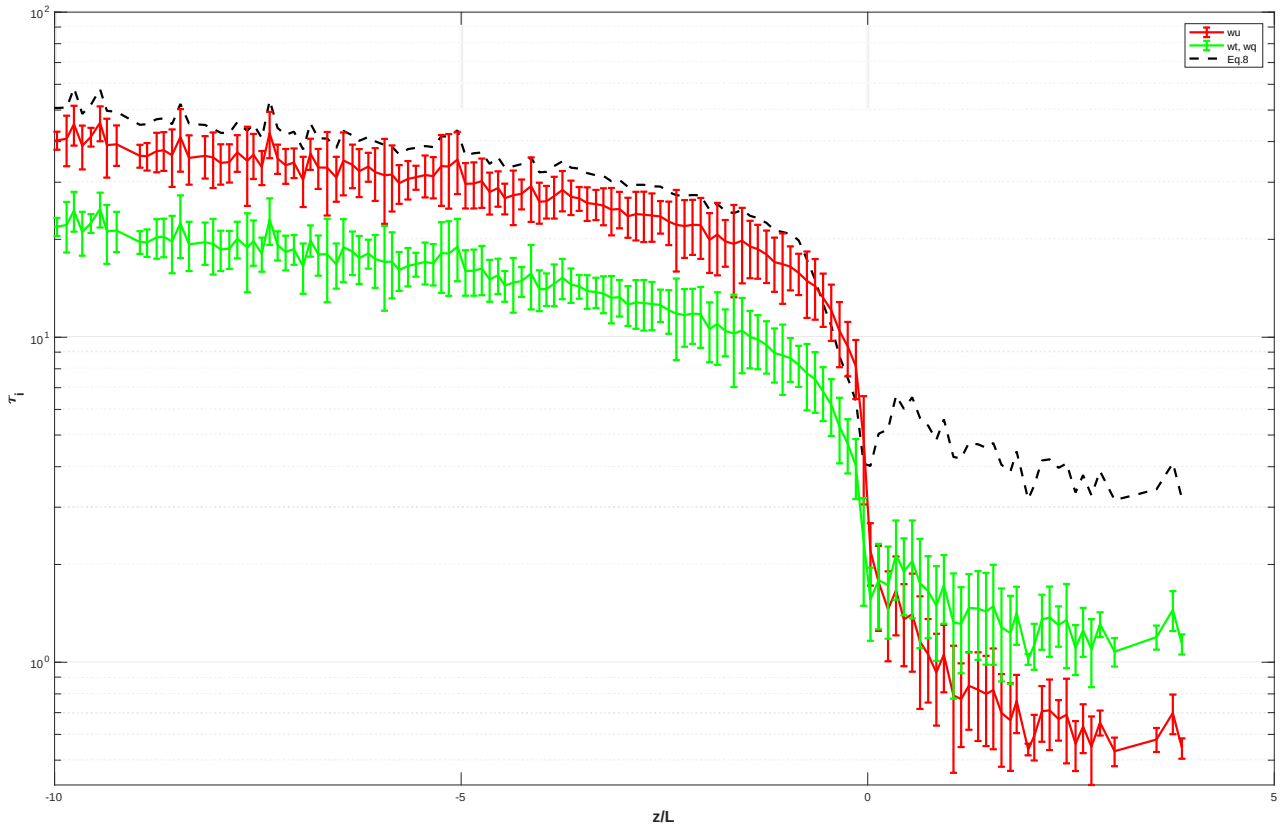

Figure 9. *Integral time scale τ averaged as a function of z/L (0.1 bins). Black dash line represent Eq. 8; red and green lines are the fitted function Eq. 11 to wu and wt, wq respectively. The errorbars represent the half-width at half-max of the distribution within the bin.*

Now that we have verified the variability of τ, we look at the assumption of joint Gaussianity. For this we select 2 field programs, Calwater and HiWinGS, and calculate directly from the raw, 10-Hz data, the first four moments, i.e. mean, variance, skewness and flatness, of the quantities *w'*, *u', t'* and *q'* and their products, *w'u', w't' and w'q'*. The variables were computed in 10-min, hourly and daily intervals. When quality criteria were not met, data were simply rejected.

Figure 10 shows the normalized probability density function (PDF) of *w'* and *u'* for a typical hour interval. Also shown are Gaussian functions with the same mean and variance. Mean values of skewness (S) and flatness (F) factors are also given in Table 2. Overall, *u'*, *t'* and *q'* are rather symmetric about their mean values, while w' appears slightly skewed (positive). Similarly the flatness of *w'* shows the largest deviation from the Gaussian value of 3.

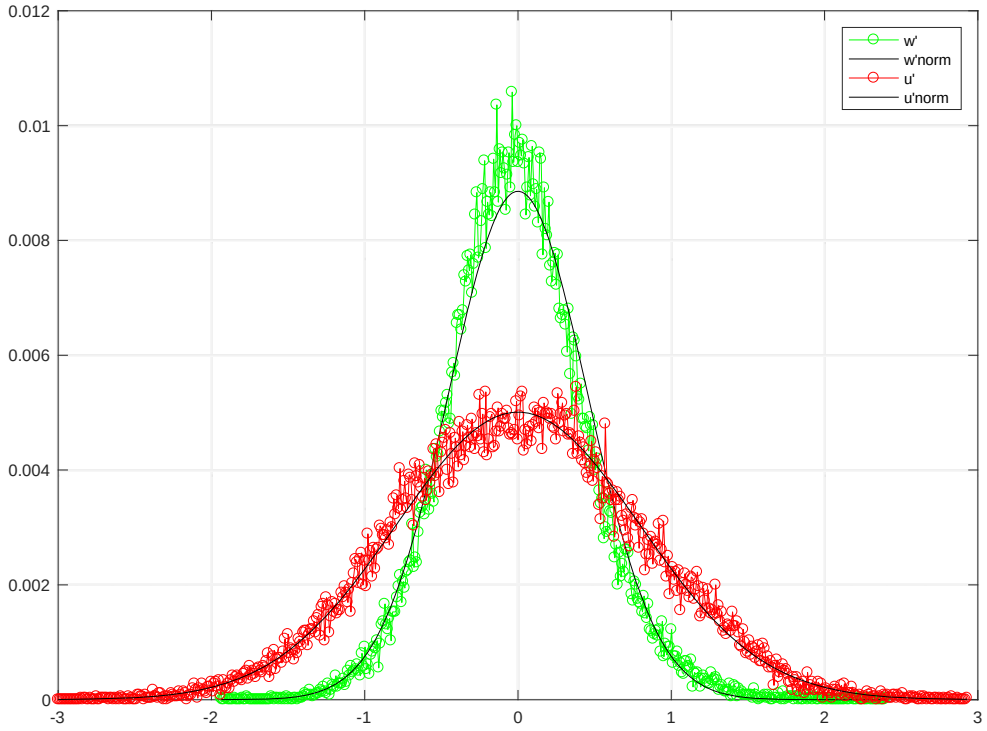

Figure 9. *Normalised probability density of w and u fluctuations for an hour in DOY21 of the Calwater project. Green- w'; red – u'; and black lines the corresponding Gaussian functions.*

Quantity	Moment	Number of data	Median	Correlation coefficient r	Gaussian values
w'	S	998	0.35	--	0
	F	998	3.74	--	3
u'	S	998	-0.02	--	0
	F	998	2.88	--	3
t'	S	998	0.11	--	0
	F	998	2.9	--	3
q'	S	998	0.01	--	0
	F	998	2.99	--	3
w'u'	S	998	-1.66	-0.27	-1.69
	F	998	12.41	-0.27	12.95
w't'	S	998	0.45	0.08	0.49
	F	998	12.63	0.08	11.11
w'q'	S	998	0.4	0.11	0.66
	F	998	12.08	0.11	10.54

Table 2. *Mean of skewness (S) and flatness (F) factor of individual quantities and their products. Also shown are the correlation coefficient r and the appropriate Gaussian values for S and F.*

Similarly we compare the measured PDF of the products to the equation used to described the joint Gaussian probability density p(x,y) (see Lu and Willmarth 1972 and Sreenivasan 1978):

$$p(x,y)=\frac{\exp[\{r/(1-r^2)\}xy]}{\pi\sqrt{(1-r^2)}}K_0\left(\frac{|xy|}{1-r^2}\right) \qquad (12)$$

with r the correlation coefficient, and K_0 the zeroth-order modified Bessel function of the second kind. From Eq. 12, we can also get the skewness as $6r + 2r^3$ and the flatness as $9 + 42r^2 + 9r^4$. Figure 11 illustrates the measured PDF for a typical hour as well as the joint PDF from Eq. 12. Measured mean values of skewness (S) and flatness (F) factors are also given in Table 2 for the products of the fluctuations. Also shown are the correlation coefficient r an the corresponding Gaussian values of S and F. Despite the fact that all stability conditions are averaged together, the results suggests that, overall, the assumption of joint Gaussianity is good for the fluctuations *w'u', w't' and w'q'* .

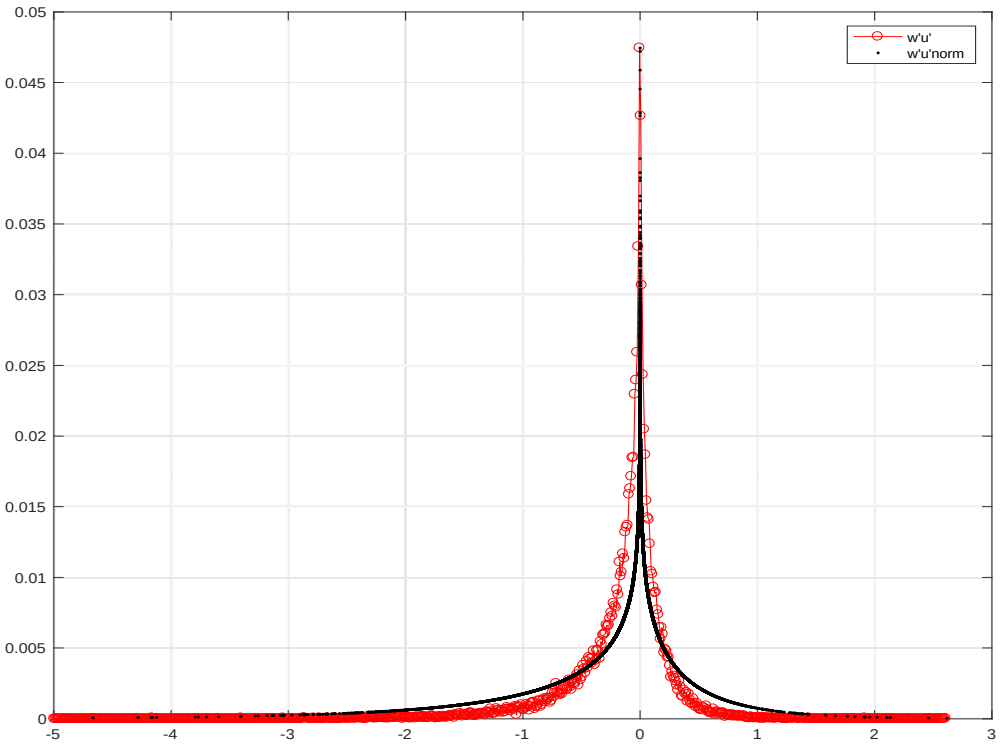

Figure 11. *Normalised probability density of product w'u' for an hour in DOY21 of the Calwater project. red – w'u' measured; black line - joint Gaussian function from Eq. 12.*

We now look at the variance of the covariance, $\sigma_{w'u'}^2$, and compare it to the products of the individual variances, σ_u^2. σ_v^2. This is similar as to comparing Eq. 5 and Eq. 9 with the noise term set to zero and using $a=\sqrt{2}$. Figure 12, left panel, shows that the approach yields a good approximation but as values

increase, the products of the variances underestimates the variance of the covariance. A better estimation is used by including the contribution of the covariance itself and is written as $\delta_{w'u'}^2=\sigma_u'^2.\sigma_v'^2+\langle w'u'\rangle^2$. This is the same approach done by Mann and Lenschow (1994) who formulated the relative error as

$$\frac{\delta_F}{|F|}=\sqrt{\frac{2\tau_i}{T}\frac{1+r^2}{r^2}} \qquad (13)$$

with the correlation coefficient r expressed $\langle x'y'\rangle/(\sigma_{x'}.\sigma_{y'})$.

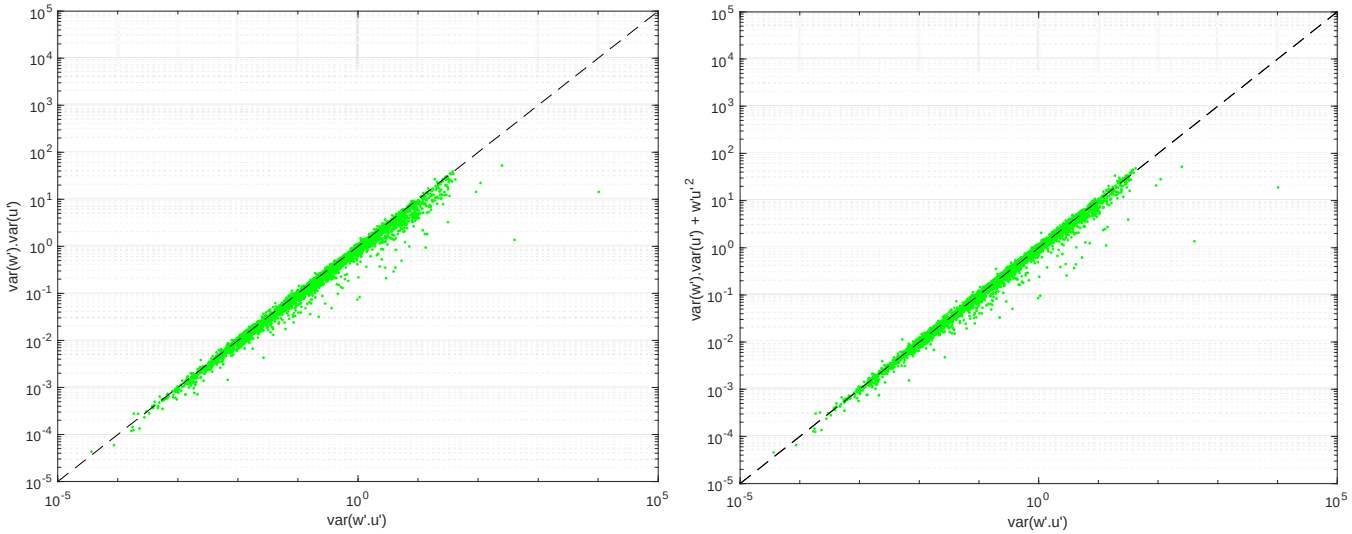

Figure 12. *Logarithmic plot of the product of the individual variance $\sigma_u'^2.\sigma_v'^2$ versus the variance of the covariance $\sigma_{w'u'}^2$ (Left panel). Right panel – same as left panel but with the covariance squared added to the product of the individual variance $\sigma_u'^2.\sigma_v'^2+\langle w'u'\rangle^2$*

With the joint Gaussianity verified, we now look at fractional flux sampling error (FFSE), which is expressed as the square root of the variance of the covariance divided by the total covariance (flux). For that we use Eq. 9 divided by the flux, with the noise term set to zero and a=1 and a=2, and Eq. 13 rewritten as:

$$FFSE=\frac{\delta_{wx}}{\overline{wx}^2}=\sqrt{\frac{2\tau_i}{T}\frac{(\overline{wx^2}-\overline{wx}^2)}{\overline{wx}^2}}=\sqrt{\frac{2\tau_i}{T}\frac{\sigma_w^2\sigma_c^2-\overline{wx}^2}{\overline{wx}^2}} \qquad (14)$$

We apply this calculation to the entire flux database and compute the error for 10-min, hourly and daily values. Figures 13 show the FFSE for the stress as a function of wind speed. Since latent heat flux is a function of wind speed and humidity, we have plotted the FFSE of latent heat fluxes as a function of air-sea humidity difference times the 10m neutral wind speed (Figure 14, top). Similarly the FFSE for sensible heat fluxes is shown as a function of air-sea temperature difference times the 10m neutral wind speed (Figure 14, bottom).

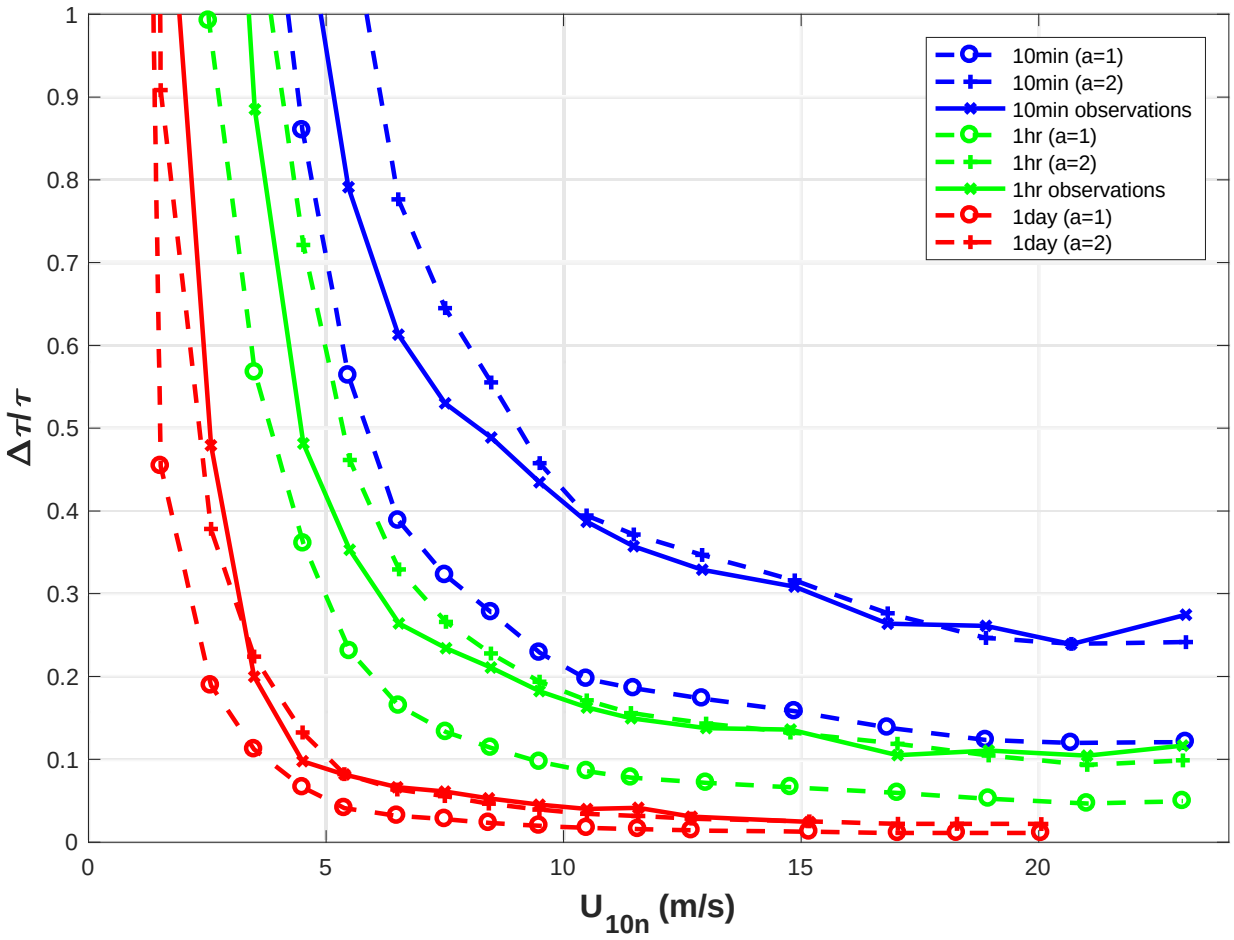

Figure 13. *Uncertainty in 10-min (blue), hourly (green) and daily (red) stress fluxes bin-averaged as a function of 10m neutral wind speed. The uncertainty for the observations is computed using Eq. 14 (solid lines). The dash lines are computed via (9) with noise set to zero and a=1 (dash line with o symbols) and a=2 (dash line with + symbols).*

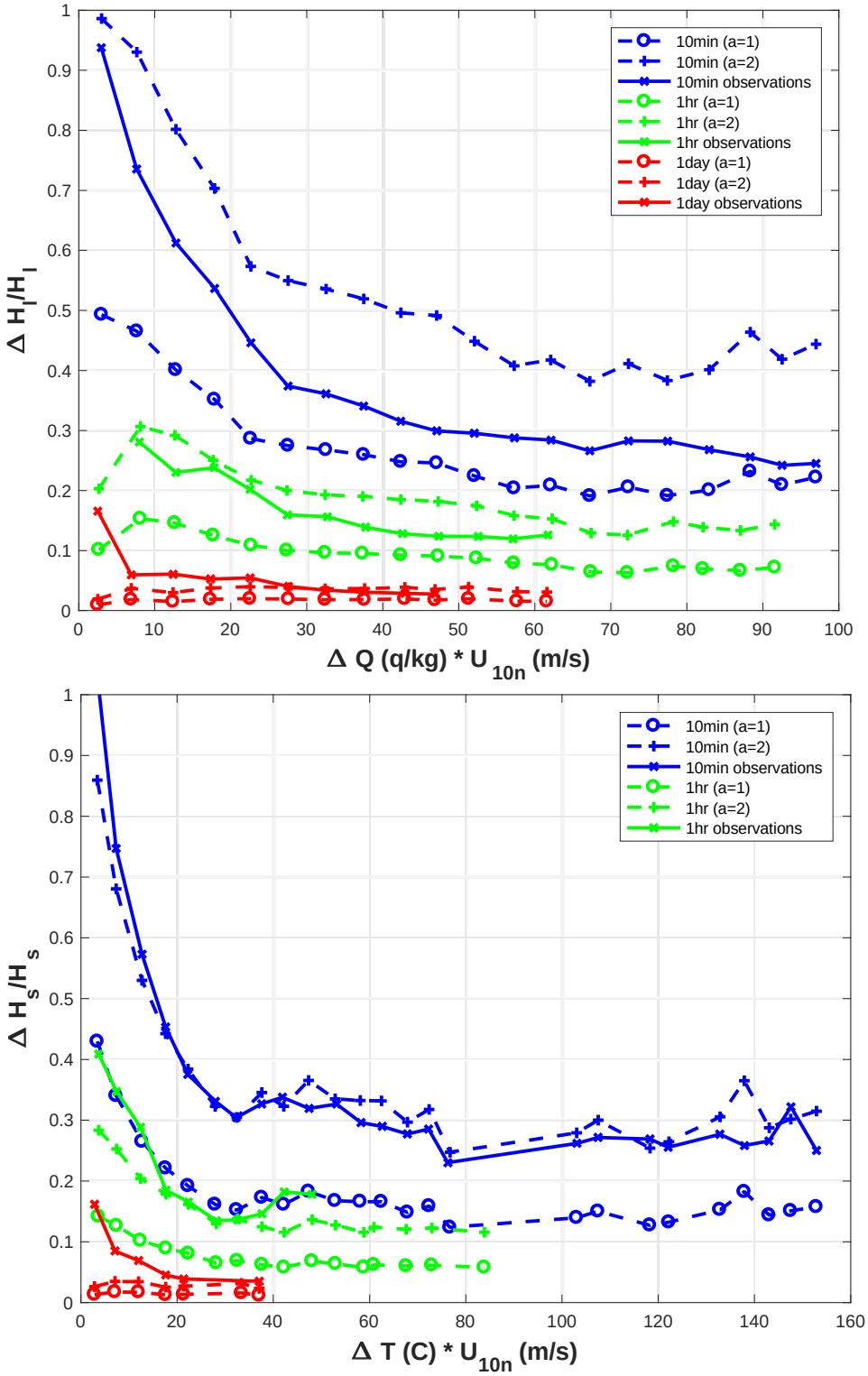

Figure 14. *Top; Same as Figure 13 but for latent heat fluxes as a function of air-sea humidity difference times the 10m neutral wind speed. Bottom; Same but for sensible heat fluxes as a function of air-sea temperature difference times the 10m neutral wind speed.*

A couple of things have to be said on Figures 13 and 14. First, the agreement between the observed error and the estimate, using a value between 1 and 2, is acceptable for all products. Most of the times a value of a=2 works better and this is what we expect from the basic definition of the FFSE.

Second, as we usually average the 10-min data to hourly values, we expect the error of the average flux to be reduced by the square-roof of 6. This is assuming there are 6 valid 10-min data points in an hour and that they are independent from one another and with the same variance. Similarly if we average hourly to daily values, it should lower the uncertainty by about a factor of 5 (the square root of 24). This is what is observed here as we see for instance the FFSE of the latent heat flux going down on average from 30% for 10-min observations to 13% for hourly data, and to 4% for daily averages.

Finally, to produce these error estimates, we have crudely averaged the 10-min individual variable variances, σ_i, to hourly and daily values. This is erroneously not taking into account the contribution of the additional correlations that will increase the uncertainty of the mean as the averaging time T increases. While for an hour average this might not be too significant, the underestimation will be quite important for longer time period like daily averages. To palliate this, an extra correlation component is usually added to the average of the variances, but we were not able to retrieve that information for the entire database. Instead we look at the 10Hz raw data set from the HiWinGS-Calwater combined example to illustrate that as our averaging period increases, the variance of the covariance will increase due to nonstationarity and/or nonhomogeneous effects creeping in.

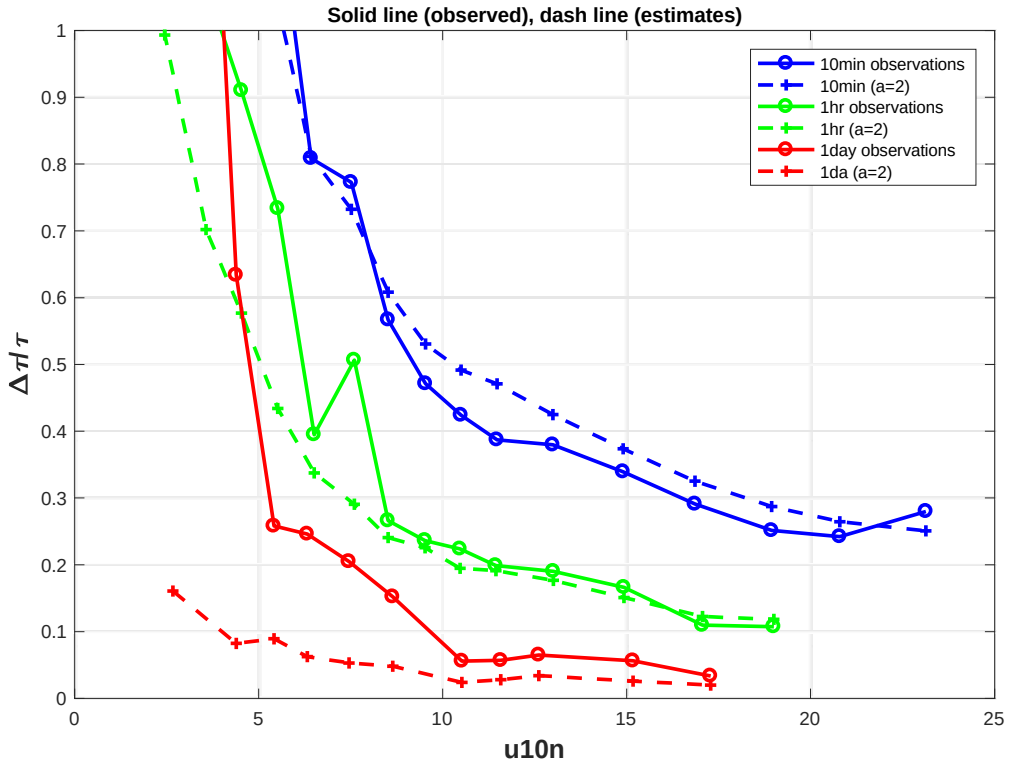

Figure 15. *Uncertainty in 10-min (blue), hourly (green) and daily (red) stress fluxes bin-averaged as a function of 10m neutral wind speed for Calwater and HiWinGS projects. The uncertainty for the observations is computed using Eq. 14 (solid lines). The dash lines are computed via (9) with noise set to zero and a=2 (dash line with o symbols).*

One can see from Figure 15 that the observed flux error is in good agreement with the 10-min estimate from Eq. 9. However there are some significant departures from the estimate at hourly and daily averages with the daily flux error showing the largest deviations from the estimated values. This highlight the fact that the variance of the covariance, and thus the random error, will decrease as our averaging time *T* increases but beyond a certain time it will rise again due to nonstationarity and/or nonhomogeneous effects.

To conclude this chapter, we note that there is also some uncertainty to our flux error estimates partly due to the noisy determination of the integral time scale τ and due to the facts that the correlation effects are not included. Any source of uncertainties is likely to produce biases (underestimation) in the uncertainty in covariance. Some authors (Finkelstein and Sims 2001, Rannik et al. 2016) reported that these error estimates could be uncertain by about 10 to 30%. A more precise approach would be to use a spectral method directly applied to the raw signal as in Lenschow and Kristensen (1985) or Finkelstein and Sims (2001).

IV) Daily spectrum of horizontal wind speed

In here we look at the spectral gap in the horizontal wind speed spectrum with frequency from 5Hz up to 1 day^{-1}. For this we use data from 6 projects, HiWings, GasEX, NEAQS, Calwater, Dynamo and WHOTS, and combine two types of data; we use 5min data to compute the power spectra up to 1day^{-1} and merge it with the power spectra usually saved during our 10-min data processing. This way we almost cover the spectral range around the gap location.
To retain only good data, we have selected time series with data coverage better than 75% to assure a descent Fourier spectrum and have rejected individual spectral amplitudes beyond the two standard deviations of all spectra. For the higher frequency 10-min spectra, we average them by wind speed bins first and then by normalized frequency bins (*fz/u*) to get a more representative average and account for the shift of spectral peak with wind speed. The final mean spectrum is then reverted back to regular frequencies.

Figure 16 shows the average normalized spectrum for each project as a function of frequency. Here we have normalized the spectra by their respective variance to account for the different conditions from one project to another and thus bring them to the same common form. Also plotted are the mesoscale model models from Larsen et al. (2015) and microscale model from Kaimal et al. (1972):

$$fS(f) = 3\ 10^{-4}\ f^{-\frac{2}{3}} + 3\ 10^{-11}\ f^{-2} \qquad \text{(Larsen)}$$

$$\frac{fS(f)}{\sigma^2} = \frac{0.164\ f/f_0}{1+0.164\ (f/f_0)^{5/3}} \qquad \text{(Kaimal)}$$

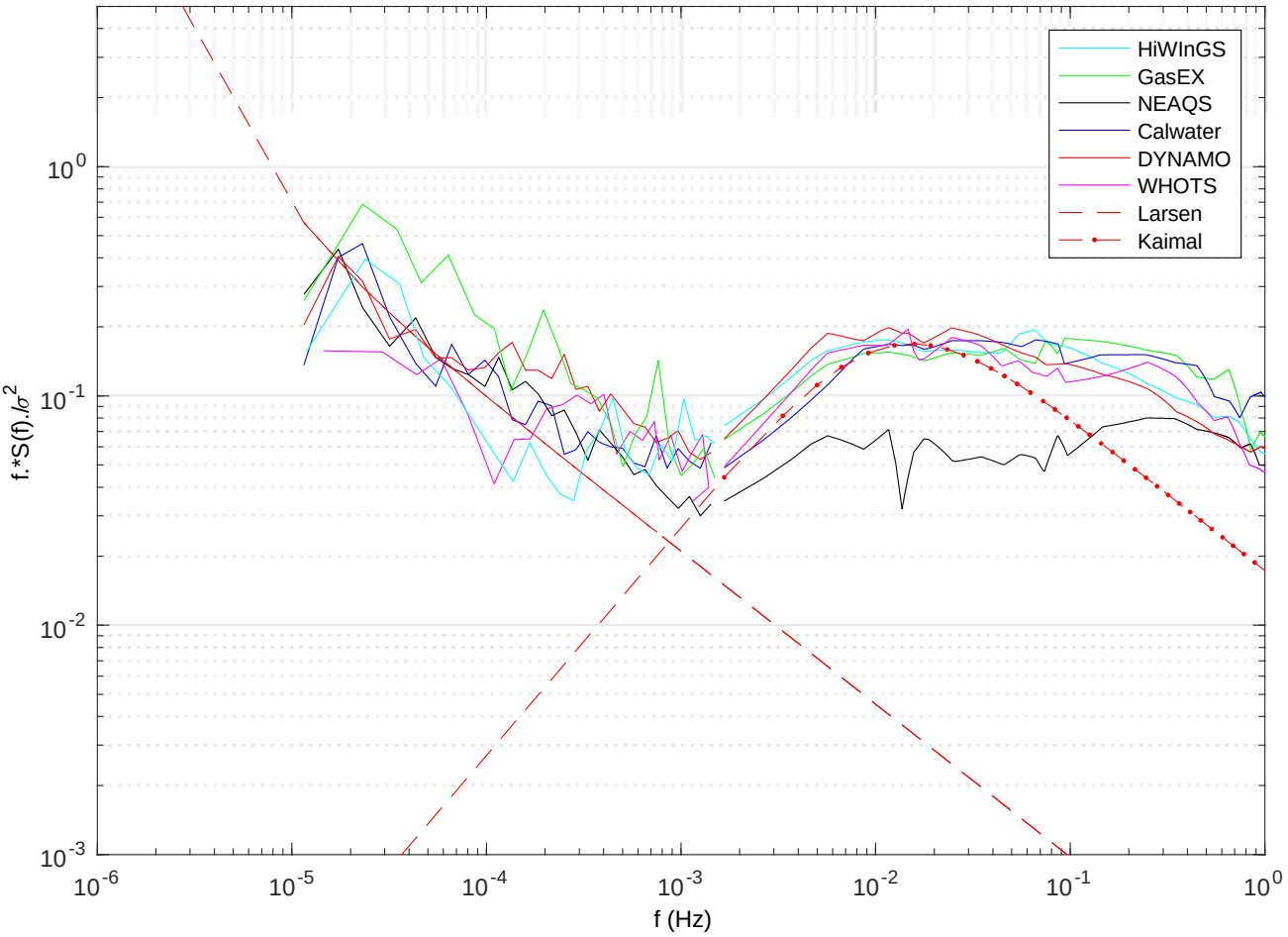

Figure 16. Normalised spectra of wind speed as a function of frequency at about 18m. Each project spectra consists of the daily spectra calculated from the 5-min time series and from the higher frequency spectra up to 10min. Also plotted are the models from Larsen (2015) scaled by a factor of 0.7, and Kaimal (1994).

We see from the figure that the spectra based on the 10-min data converge rather nicely with the spectra made from the 5-min time series. The high frequency spectrum from NEAQS is lower probably reflecting that the shallower boundary layer conditions. Nevertheless the microscale power energy is still strong enough to visualize the gap.

For all spectra, the spectral transition from the microscale (boundary-layer turbulence) to mesoscale (external fluctuations) suggests on average a gap when f is close to 10^{-3} Hz (17min^{-1}). For spatial scales larger than the gap, the spectra decrease with frequency with a -2/3 slope roughly. For frequencies above the gap, the spectra follow the f^{+1} shape of the Kaimal spectrum. This suggests that the observations can be decomposed as a linear superimposition of mesoscale and microscale variations leading to a weak correlation between the two components (Larsen et al. 2015). It is because of the existence of this gap that we can analyze the time series through statistically stationary theories and models. On average our data show a gap at about 17min^{-1} but others have reported gap in the $30\text{-}60\text{min}^{-1}$ spectral range (Larsen et al. 2015). This reveals that when we compute hourly fluxes, we have reached the stationarity limit and

probably include some macroscale fluctuations to our statistics, like in the random error computations for instance (see previous chapter III).

V) Gustiness as a function of time scale

The gustiness term is reported in Fairall et al (1996a) and Cronin et al. (2006) as a missing variance due to the difference between using a scalar average S and a vector average u^2. As the averaging time increases, mesoscale effects will contribute more to the missing variance and thus we use an equation similar as in Cronin et al. (2006) to look at this with our dataset. We express the average value of the wind speed S as the sum of the vector wind speed u^2 plus a convective gustiness u_g^2 and a mesoscale gustiness u_{meso}^2.

$$S^2 = u^2 + u_g^2 + u_{meso}^2 = u^2 + (\beta W_*)^2 + u_{meso}^2 \qquad (15)$$

with W_* the convective scaling velocity defined as $W_* = \left(\frac{gz_i}{T}\overline{w'\theta'_v}\right)^{1/3}$, and β an empirical constant which depends on the temporal/spatial scale used to compute the averages.

Similarly to the approach in Fairall et al. (1996a) we first start to compute β by using the horizontal velocity variances at different time scale. For this exercise, we use our 10-min dataset and assume that the variables are independent from one another and thus average them to the desired time scale, hourly to 1day. For 10-min we find a value of 1.3 which is close to 1.25 used in the COARE algorithm. Then the constant increases with time and level off at some point to a value of about 1.5.

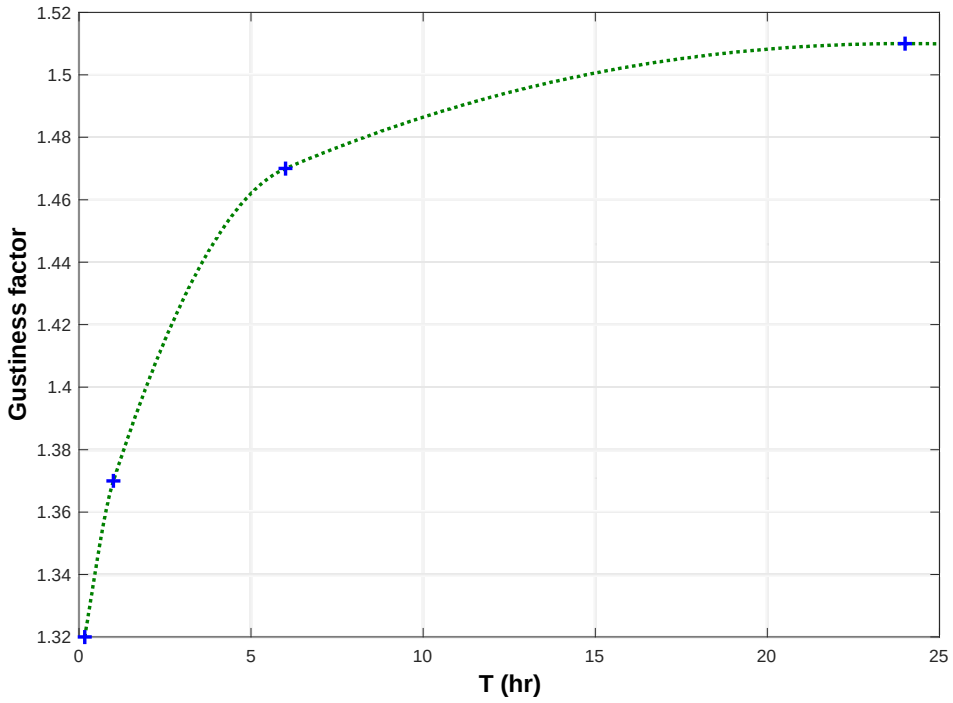

Figure 17. Gustiness constant versus time scale.

We note here that we are most likely underestimating the β constant, as a simple average of the variance with time is erroneous. Moreover the mesoscale gustiness might not scale well with W_*. Thus we compute the difference between the scalar and vector wind speed to look at the combined mesoscale and gustiness effects for a daily average. We plot the result as function of latitude on Figure 18. We see that the difference is more pronounced for a daily average as well as for higher latitudes.

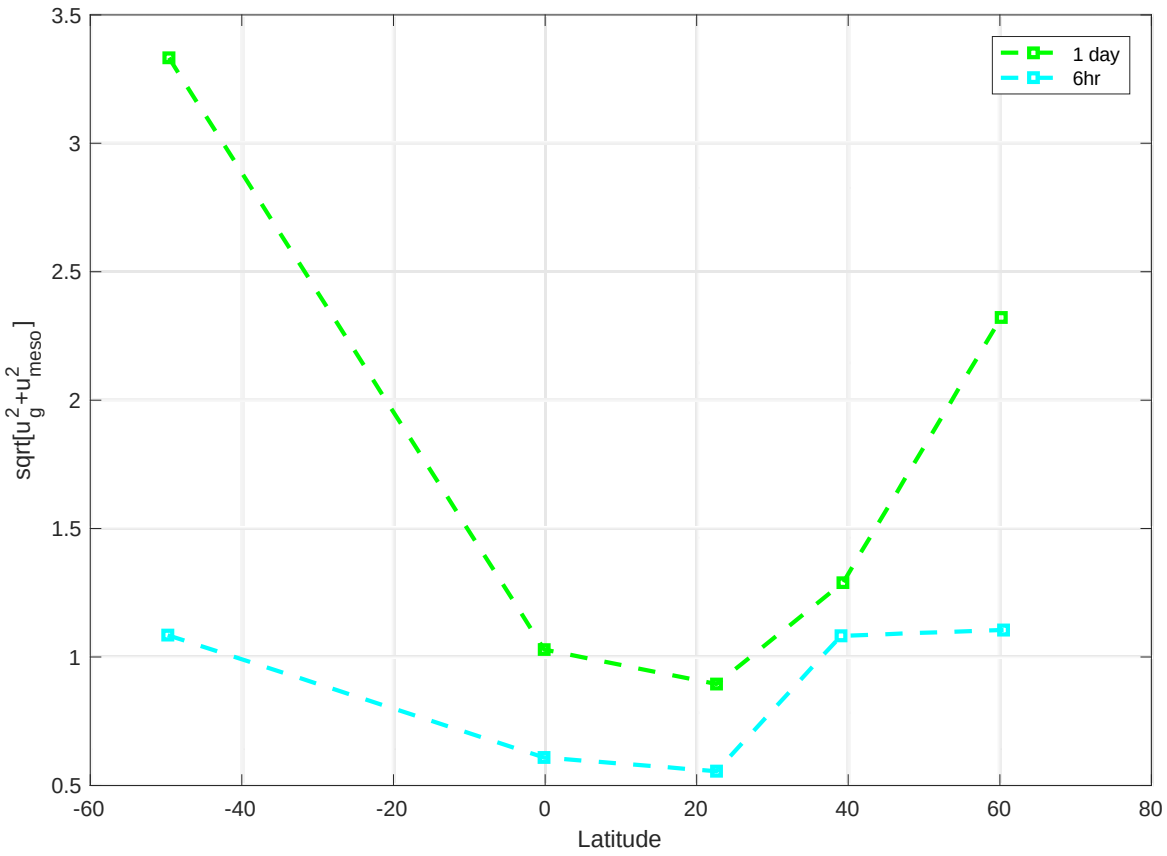

Figure 18. Mesoscale and convective gustiness as a function of latitude for daily (green) and 6-hr averages (cyan).

If we apply this correction to a daily bulk flux computation, we can see that the bias introduced by a vector daily averaged wind speed is greatly reduced. Figure 19 shows the difference if we consider the mesoscale correction and it improves the one-to-one ratio of the daily stress computed from daily averaged state variables and the daily stress computed form 10-min data. Figure 20 is similar but here we plot the difference of the two versus latitude.

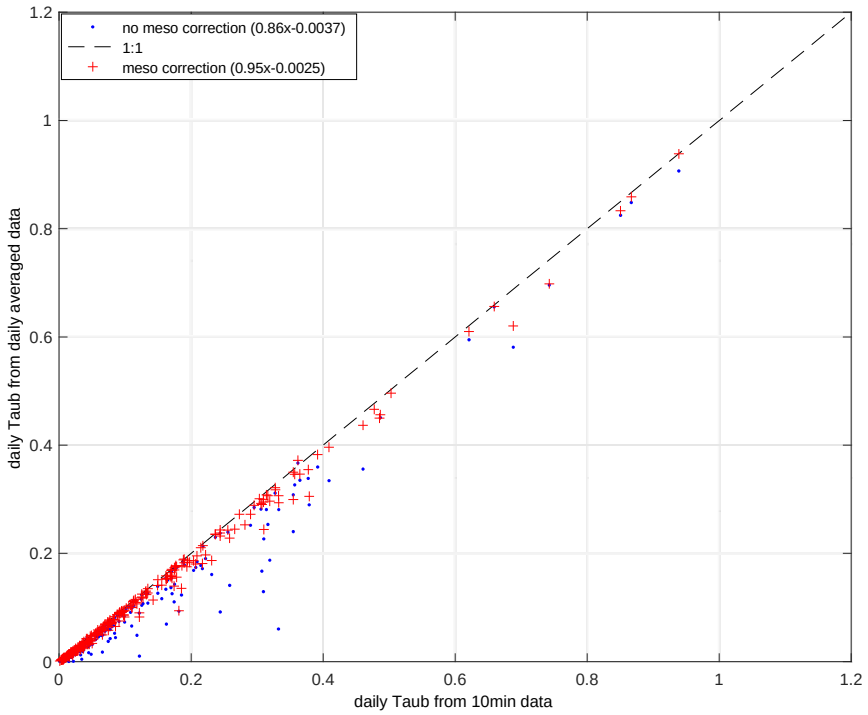

Figure 19. Daily stress computed from daily averaged state variables versus daily stress computed form 10-min data; blue dots – without any mesoscale gustiness correction; red crosses – with a mesoscale correction.

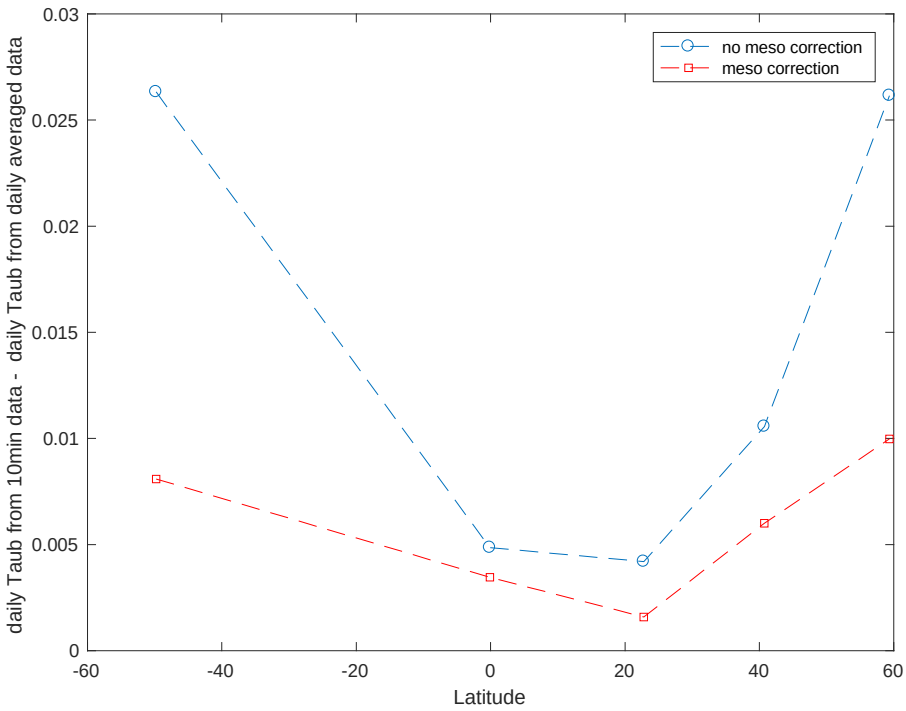

Figure 20. Mean difference between the daily stress computed form 10-min data and the daily stress computed from daily averaged state variables as a function of latitude; blue line – without any mesoscale gustiness correction; red line– with a mesoscale correction.

VI) Wind Distributions

The distribution of wind speed is usually well-fit by a Weibull distribution (See Panoksky and Dutton, p 332).

$$p(U) = \frac{b}{a}(\frac{U}{a})^{b-1} \exp[-(\frac{U}{a})^{b}] \quad (17)$$

The moments of this distribution are:

$$\overline{U^n} = a^n * \Gamma(1+n/b) = (\overline{U})^n \frac{\Gamma(1+n/b)}{\Gamma(1+1/b)} \quad (18)$$

The mean and standard deviation are given by:

$$\overline{U} = a\Gamma(1+1/b) \quad (19)$$

$$\sigma_u = a\left[\Gamma(1+2/b) - \Gamma(1+1/b)\Gamma(1+1/b)\right]^{1/2} \quad (20)$$

The recent paper (Monahan 2006a) gives more information about oceanic wind distributions. He shows that in the Southern Ocean region, b=3; thus a=1.11*$\overline{U}$ and $\sigma_u = \overline{U}/3$. On an annual average, $\overline{U}$ is about 11 m/s.

One handy property of the Weibull distribution is the cumulative probability that U exceeds some selected threshold, U', is simply

$$\Pr ob(U > U') = \exp[-\left(\frac{U'}{1.11\overline{U}}\right)^{b}] \quad (21)$$

Here we apply the distribution to the flux base and divide the data into 3 groups: tropical (-15 to +15 deg latitude), subtropical (15<abs(lat)<40 deg), and high latitude (40<abs(latitude)<90 deg).

The tropical and subtropical gave essentially the same results so they were combined together (Fig. 21a). The high latitude result is shown in Fig. 21b. The Weibull parameters are roughly consistent with Monahan. The low latitudes show more extreme winds than Weibull but the high latitude is about the same.

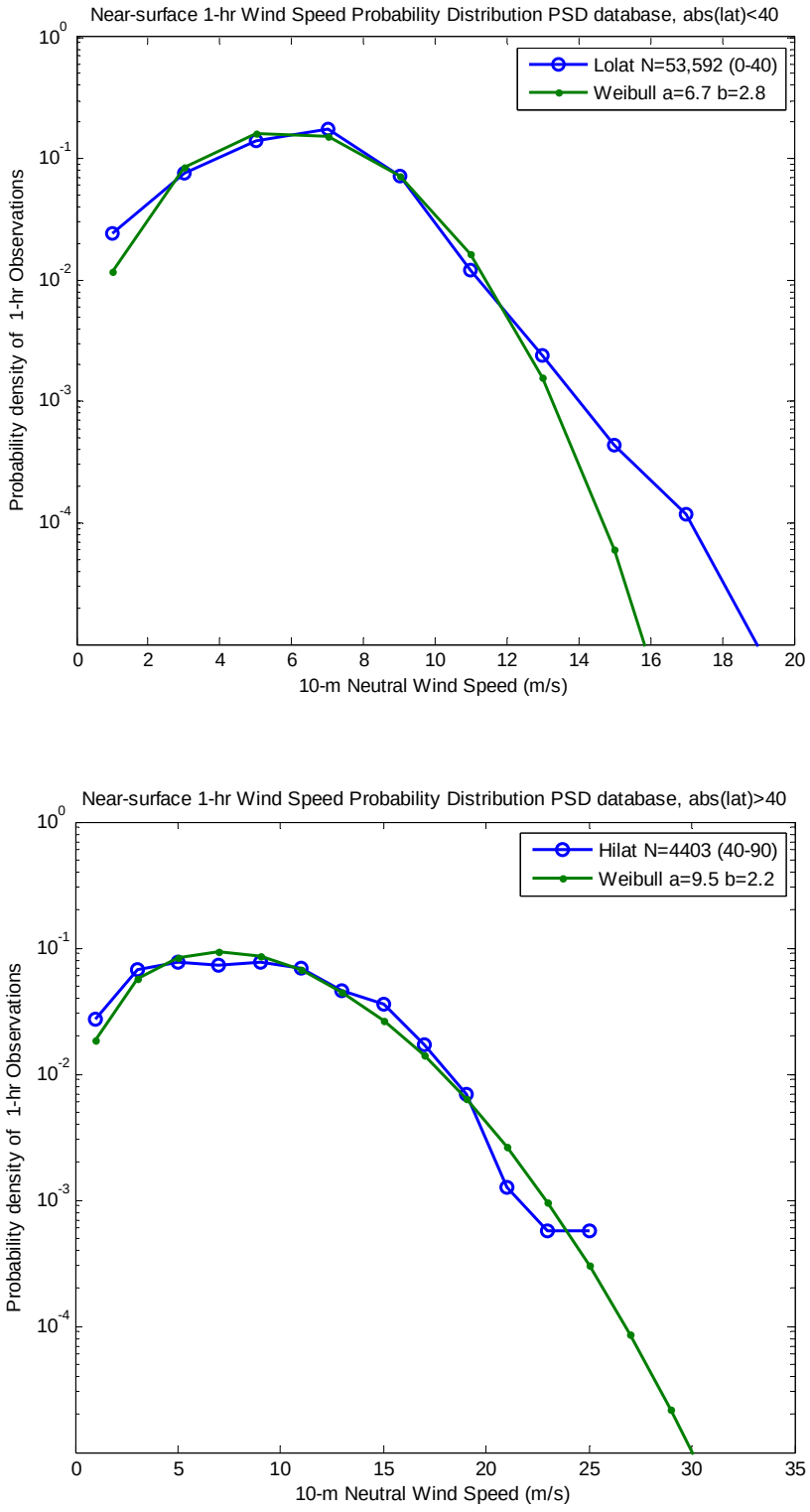

Figure 21. *Probability density distributions of 1-hr values U10n for the PSD flux database. Upper panel: abs(latitude)<40. Lower panel: abs(latitude>40). The green line is a Weibull distribution fit (parameters given in the legend).*

REFERENCES

Blomquist B. W., B. J. Huebert, C. W. Fairall and I. C. Faloona. 2010: Determining the sea-air flux of dimethylsulfide by eddy correlation using mass spectrometry. Atmos. Meas. Tech., 3 (1), 1-20. doi:10.5194/amt-3-1-2010

Cronin, M. F., C. W. Fairall, and M. J. McPhaden. An assessment of buoy-derived and numerical weather prediction surface heat fluxes in the tropical Pacific. J. Geophys. Res., 111, C06038, doi:10.1029/2005JC003324, 2006.

Edson, J.B., and Coauthors, 2013: On the exchange of momentum over the open ocean. J. Phys. Oceanogr., 43, 1589–1610, doi:10.1175/ JPO-D-12-0173.1.

Fairall, C. W., E. F. Bradley, J. S. Godfrey, G. A. Wick, J. B. Edson, and G. S. Young (1996a), Cool-skin and warm-layer effects on sea surface tempera- ture, J. Geophys. Res., 101, 1295 – 1308.

Fairall, C. W., Hare, J. E., Edson, J. E., and McGillis, W.: Parameterization and micrometeorological measurement of air-sea gas transfer, Bound. Lay. Meteorol., 96, 63–105, 2000.

Fairall, C. W., L. Bariteau, A. A. Grachev, R. J. Hill, D. E. Wolfe, W. A. Brewer, S. C. Tucker, J. E. Hare, andW. M. Angevine (2006), Turbulent bulk transfer coefficients and ozone deposition velocity in the International Consortium forAtmospheric Research into Transport and Transformation, J. Geophys. Res., 111, D23S20, doi:10.1029/2006JD007597.

Fairall, C. W., E. F. Bradley, J. E. Hare, A. A. Grachev, and J. B. Edson, 2003: Bulk parameterization of air–sea fluxes: Updates and verification for the COARE algorithm. J. Climate, 16, 571–591, doi:10.1175/1520-0442(2003)016,0571: BPOASF.2.0.CO;2.

Finkelstein, P. L. and Sims, P. F.: Sampling error in eddy correlation flux measurements, J. Geophys. Res., 106, 3503–3509, 2001.

Fratini, G., D. K. McDermitt, and D. Papale, 2014: Eddy-covariance flux errors due to biases in gas con- centration measurements: origins, quantification and correction, *Biogeosciences*, 11, 1037–1051.

Kaimal, J., Wyngaard, J., Izumi, Y., and Cote´, O.: Spectral characteristics of surface-layer turbulence, Q. J. Roy. Metor. Soc., 98, 563–589, 1972.

Larsén, X.G., Larsen, S.E. & Petersen, E.L. Boundary-Layer Meteorol (2016) 159: 349. doi:10.1007/s10546-016-0129-x

Lenschow, D. H. and Kristensen, L.: Uncorrelated noise in turbu- lence measurements, J. Atmos. Ocean. Tech., 2, 68–81, 1985.

Lu, S. S. and Willmarth, W. W.: 1972, 'The Structure of the Reynolds Stress in a Turbulent Boundary Layer', Tech. Report 021490-2-T, Department of Aerospace Engineering, Gas Dynamics Laboratories, The University of Michigan.

Lumley, J.L., and H. A. Panofsky, The Structure of Atmospheric Turbulence 239pp.,Wiley-Interscience, NewYork,1964.

Mann, J., and D. H. Lenschow, Errors in airborne flux measurements, J. Geophys. Res., 99, 14,519-14,526, 1994.

Monahan, A. H., 2006a: The probability distribution of sea surface wind speeds. Part I: Theory and SeaWinds observations. J. Climate, 19, 497–520, doi:10.1175/JCLI3640.1.

Nakai T., K. Shimoyama, Ultrasonic anemometer angle of attack errors under turbulent conditions, Agric. Forest Meteorol., 162 (2012), pp. 14–26

Panofsky, H. A., Dutton, J. A., 1984: Atmospheric Turbulence. New York: John Wiley & Sons, 397pp.

Rannik, Ü., Peltola, O., and Mammarella, I.: Random uncertainties of flux measurements by the eddy covariance technique, Atmos. Meas. Tech., 9, 5163-5181, doi:10.5194/amt-9-5163-2016, 2016.

Sreenivasan,K. R., A. J. Chambers, and R. A. Antonia, Accuracy of Moments of velocity and scalar fluctuations in the atmospheric surface layer, Boundary Layer Meteorol.,14, 341-359, 1978.

Wyngaard, J. C.: On surface-layer turbulence, Workshop on Micrometeorology, edited by: Haugen, D. A., American Meteorol- ogy Society, 101–149, 1973.